Red Fluorescent Proteins: Advanced Imaging Applications and Future Design
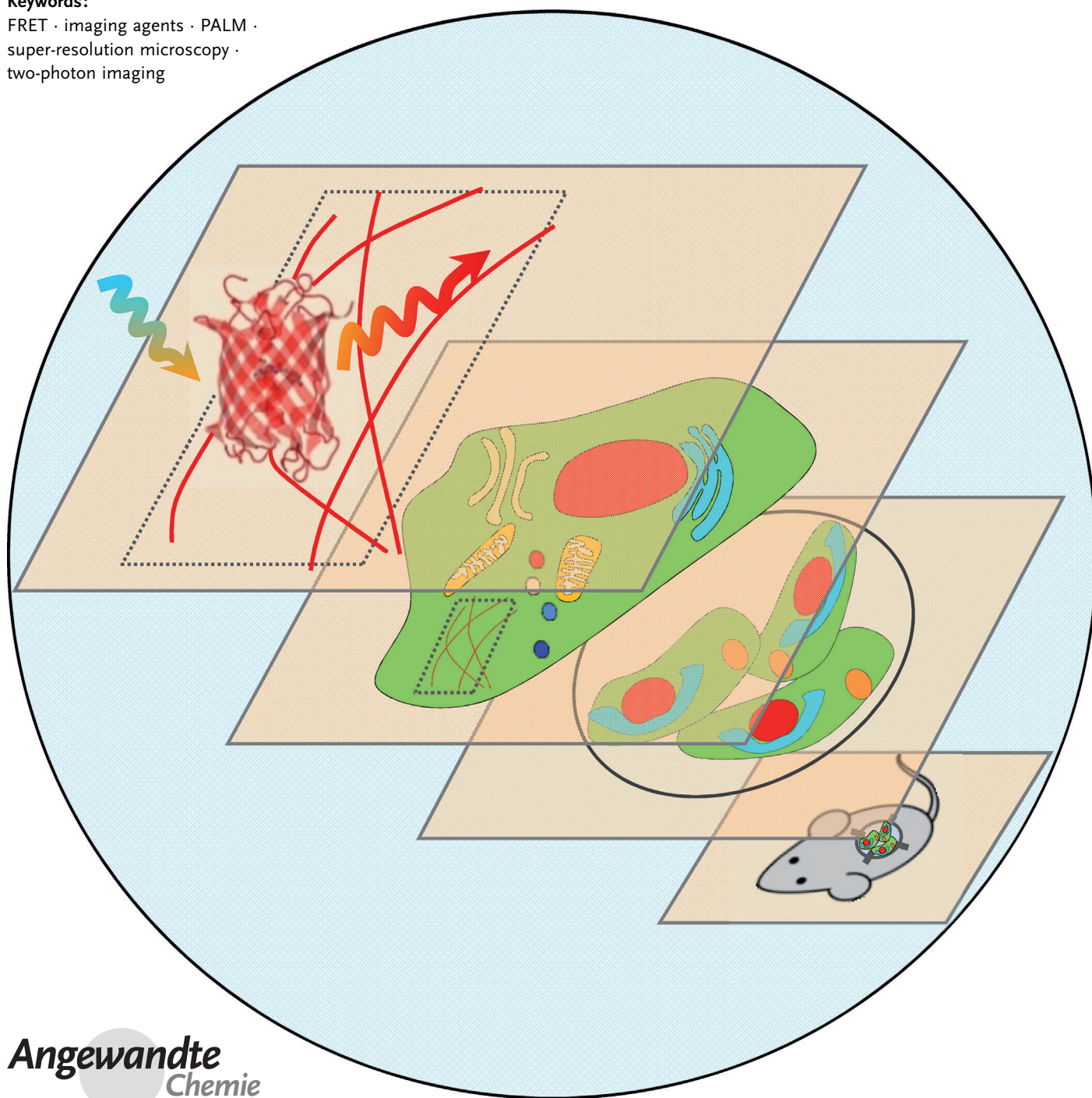
Daria M. Shcherbakova, Oksana M. Subach, and Vladislav V. Verkhusha*

Angewandte
Chemie

In the past few years a large series of the advanced red-shifted fluorescent proteins (RFPs) has been developed. These enhanced RFPs provide new possibilities to study biological processes at the levels ranging from single molecules to whole organisms. Herein the relationship between the properties of the RFPs of different phenotypes and their applications to various imaging techniques are described. Existing and emerging imaging approaches are discussed for conventional RFPs, far-red FPs, RFPs with a large Stokes shift, fluorescent timers, irreversibly photoactivatable and reversibly photoswitchable RFPs. Advantages and limitations of specific RFPs for each technique are presented. Recent progress in understanding the chemical transformations of red chromophores allows the future RFP phenotypes and their respective novel imaging applications to be foreseen.

From the Contents

1. Introduction

Genetically encoded fluorescent proteins (FPs) allow the specific and targeted labeling of proteins, organelles, cells, tissues, and whole organisms. This versatility makes FPs superior over synthetic organic dyes for imaging applications in vivo. Once expressed in cells, FPs require no additional enzymes and cofactors except for molecular oxygen to form a chromophore. In most cases, a protein of interest can be genetically tagged with FP without affecting its function and delivered into live cells. Fluorescent organic dyes (reviewed in Ref. [1]) have several advantages over FPs. These include their small size that ensures low interference with the function of a labeled protein, and sometimes they have more-favorable photophysical characteristics, such as greater brightness or higher photostability. However, use of organic dyes is usually limited to fixed cells. Modern FPs of new phenotypes and with enhanced photophysical properties allow efficient imaging applications in live cells.

FPs are available in a range of fluorescent colors, which span the whole visible spectrum, from short violet to far-red. Red-shifted FPs (RFPs) complement other spectral FP variants in multicolor applications and present a number of advantages. Specifically, red-shifted excitation and fluorescence result in reduced autofluorescence, lower light-scattering, and lower phototoxicity at longer wavelengths. These properties make RFPs superior probes for in vivo imaging, particularly, in deep tissues and for imaging approaches that require low background noise including single-molecule super-resolution techniques.

Designing FPs to satisfy the needs of novel imaging technologies is a rapidly developing area. Recently, many RFPs of different phenotypes have been engineered. Currently, there are at least six different RFP types, including conventional RFPs, far-red FPs, RFPs with a large Stokes shift, fluorescent timers, photoactivatable RFPs, and reversibly photoswitchable RFPs. Each of these phenotypes enables different imaging application.

The variety of FP colors originates from the diversity of the chromophores and their immediate environments. Development of advanced RFPs has been accompanied with studies of the corresponding chromophore structures and their formation processes.[2] As a result, the basic principles of the autocatalytic and light-induced chemistry of the red chromophore are now known. Understanding the chromophore chemistry opens a possibility to manipulate transitions between chromophore structures to obtain desirable FP phenotypes.

In this Review, we first describe existing and emerging applications of RFPs including techniques to study protein–protein interactions, to monitor intracellular dynamic processes, and to perform intravital and super-resolution imaging. Required FP characteristics are discussed for each imaging approach. We then summarize the principles of the chromophore transformations in RFPs. Finally, we present our view on a design of future RFPs and their influence on imaging applications.

2. Conventional Red-Shifted FPs

Permanently fluorescent, or so-called conventional RFPs, can be divided into orange FPs (emission at 550–570 nm), red FPs (emission at 570–620 nm), and far-red FPs (emission at over 620 nm) on the basis of their spectral properties. Far-red shifted RFPs are discussed separately to highlight their importance for imaging.

[*] Dr. D. M. Shcherbakova,[+] Dr. O. M. Subach,[+] Dr. V. V. Verkhusha
Department of Anatomy and Structural Biology and Gruss-Lipper Biophotonics Center
Albert Einstein College of Medicine
1300 Morris Park Avenue, Bronx, NY 10461 (USA)
E-mail: vladislav.verkhusha@einstein.yu.edu

[+] These authors contributed equally to this work.

Major spectral and biochemical properties of RFPs are summarized in Table 1. These characteristics include brightness, photostability, oligomeric state, maturation (protein folding and chromophore formation) rate, and cytotoxicity. Brightness of FP is determined as a product of its extinction coefficient and its quantum yield. In cells, however, in addition to the FP's intrinsic brightness, the maturation efficiency of FP and the level of its expression, both influence the apparent brightness of the fluorescent signal. Other RFP characteristics are defined in the footnotes to Table 1.

The FP cytotoxicity determines its suitability for cell labeling. The absence of the cytotoxicity ensures the constant and high-level of the FP expression, high cell viability, and efficient cell division over a large number of cell generations. The cytotoxicity may be caused by a non-specific intracellular FP oligomerization and formation of large aggregates.[3] Through the optimization of the protein solubility less-cytotoxic variants could be prepared, even for tetrameric RFPs, such as DsRed.[3a, 4] The cytotoxicity can be evaluated in bacterial cells by determining an average colony size and the number of colonies after constitutive high-level FP expression. In mammalian cells expressing FP under a strong promoter, the cytotoxicity can be determined by monitoring the level and distribution of cellular fluorescence over several cell generations.[3a] Tetrameric E2-Orange and DsRed-Express2 have been optimized in this way.[3a, 5]

Modern RFPs have enhanced characteristics compared to the first generation of conventional RFPs. mOrange2 and TagRFP-T[6] proteins are substantially more photostable (Table 1) than their ancestors mOrange[7] and TagRFP.[8] Other orange FPs, such as mKO2[9] and mKOk,[10] are brighter and have faster maturation times, however, they still suffer from low photostability. A new RFP, called mRuby,[11] is characterized by higher brightness (Table 1). For comparison, the brightness of the orange-red synthetic Alexa dyes is 88 mM^{-1}cm^{-1} for Alexa546 and 61 mM^{-1}cm^{-1} for both Alexa568 and Alexa594.[1b] Correlating that with the brightness of RFPs with similar spectral characteristics (Table 1), Alexa546 is 1.4-times brighter than mKOk, Alexa568 is 1.6-times less-bright than tdTomato, and Alexa594 is 1.6-times brighter than mRuby.

Although the new RFPs offer advantages for specific applications some earlier RFPs are still competitive. The popular mCherry[7] protein is often a label of choice because of its high photostability and good performance in fusion constructs with other proteins. In a number of applications, such as organelle labeling and Förster resonance energy transfer (FRET), the bright tandem dimer tdTomato[7] provides optimal results.

2.1. RFPs in Biosensors and Bimolecular Fluorescence Complementation

Genetically encoded biosensors allow the visualization and quantification of the changes in enzymatic activities, in protein conformational states, in concentrations of metabolites and in some other physiological events in cells, tissues, and whole organisms.[12] Since red-shifted light penetrates deeper into tissues and provides lower levels of autofluorescence, RFPs are attractive components for biosensors for use in tissues and model animals.

There are two major types of FP biosensors: FRET-based biosensors and single-FP biosensors. A design of spectrally compatible FRET biosensors for the simultaneous imaging of multiple biological processes in a single cell is a current trend in the FP area.[13] When used as FRET acceptors, mKO2 and mKOk with their fast and efficient maturation demonstrated high FRET efficiency with cyan–green FP donors.[10, 14] These proteins would be also good FRET donors to be combined with far-red FP acceptors. The resulting FRET pairs could be compatible with the common cyan FP (CFP)-yellow FP (YFP) FRET pair.

Single-FP biosensors are based on FPs, which reversibly change their spectra upon specific stimuli (Figure 1b, Table 2). These biosensors have been developed to detect pH changes, concentrations of chloride and metal ions, and redox potential. The main advantage of the single-FP over the FRET-based biosensors is the substantially higher dynamic range of their readout.[15] The majority of single-FP biosensors are green. Very few red single-FP sensors, such as a biosensor for detection of nucleoside transport based on pH-sensitive mNectarine,[16] are currently available. Future engineering of orange–red single-FP sensors could allow detecting simultaneously several processes in a live cell.

Recently, considerable progress in the biosensor design has been made with a new approach to screen bacterial colonies expressing fluorescent probes in the periplasm. As

Daria Shcherbakova received her M.S. in Chemistry in 2005 and Ph.D. in Bioorganic Chemistry in 2009, both from the School of Chemistry of Moscow State University. In 2010 she joined the laboratory of Dr. Verkhusha as a postdoctoral research fellow. Her research interests focus on the design of fluorescent probes and molecular biosensors and their applications.

Oksana Subach received her M.S. in Chemistry in 1996 and Ph.D. in Bioorganic Chemistry in 2000, both from the School of Chemistry of Moscow State University. She obtained her postdoctoral training in the Department of Chemistry of Natural Compounds of the same School in Moscow and, from 2007, in the Department of Anatomy and Structural Biology of the Albert Einstein College of Medicine in New York. Her research interests include the engineering and applications of advanced fluorescent proteins and studying the mechanisms of their chromophore transformations.

a result, a series of blue, green, and red calcium ion biosensors with the dynamic ranges of 1000–11 000 % were obtained.[17] These biosensors were based on circularly permutated FPs (cpFPs), which have new N- and C- termini in the middle of the β-barrel. The red calcium biosensor, based on circularly permutated mApple, was applied together with a CFP–YFP probe for adenosine 5′-triphosphate for simultaneous imaging in a single cell.

In addition to common biosensors, split variants of conventional RFPs are utilized for the detection of protein–protein interactions in bimolecular fluorescent complementation (BiFC) assay.[18] Split FPs are composed of two non-fluorescent FP parts that reconstitute a fluorescent FP barrel when brought in close proximity (Figure 1c, Table 2). Usually BiFC is irreversible, and it takes time to form a mature chromophore in the reconstituted FP molecule. However, sometimes it is more preferable than a FRET-based assay because of its simplicity and sensitivity. Among RFP-based split systems available, only mKate derivative split-Lumin can mature efficiently in physiological conditions at 37 °C, and can be combined with split FPs of other colors.[18b]

Another method was utilized to develop an FP-based approach for reporting a cell-cycle phase. Sequential expression of two different FP fusion constructs, such as mKO2 fused to Cdt1 and mAG fused to Geminin, has resulted in a Fucci biosensor system.[9] Due to cell-cycle-dependent proteolysis, protein expression of Cdt1 and Geminin oscillates inversely. Hence, mKO2–hCdt1 labels the nuclei in orange during G1 phase, while mAG–hGem labels the nuclei in green during S/G2/M phases. Fucci allowed the coordination of the cell cycle with morphological changes in neural progenitors[19] and cell-cycle progression during differentiation, metastasis of tumors,[9] and the development of zebrafish embryo to be studied.[20]

2.2. RFPs in Deep Tissue Imaging

Non-destructive imaging of thick specimens, including live ones, requires optical sectioning to eliminate out-of-focus light. This sectioning could be achieved using fluorescence light-sheet microscopy and two-photon (2P) imaging, among other approaches.

Vladislav Verkhusha received his M.S. in Biophysics from the Moscow University of Physics and Technology and his Ph.D. in Chemical Kinetics and Catalysis from the Moscow State University. He obtained post-doctoral training in the Osaka Bioscience Institute and in the research centers of Japan Science and Technology Corporation in Kyoto and Tokyo. In 2002 he was appointed assistant professor at the University of Colorado. From 2006 on he has been associate professor and then professor at the Albert Einstein College of Medicine in New York. His research interests include the development of fluorescent probes, biosensors, high-throughput screening, and imaging approaches.
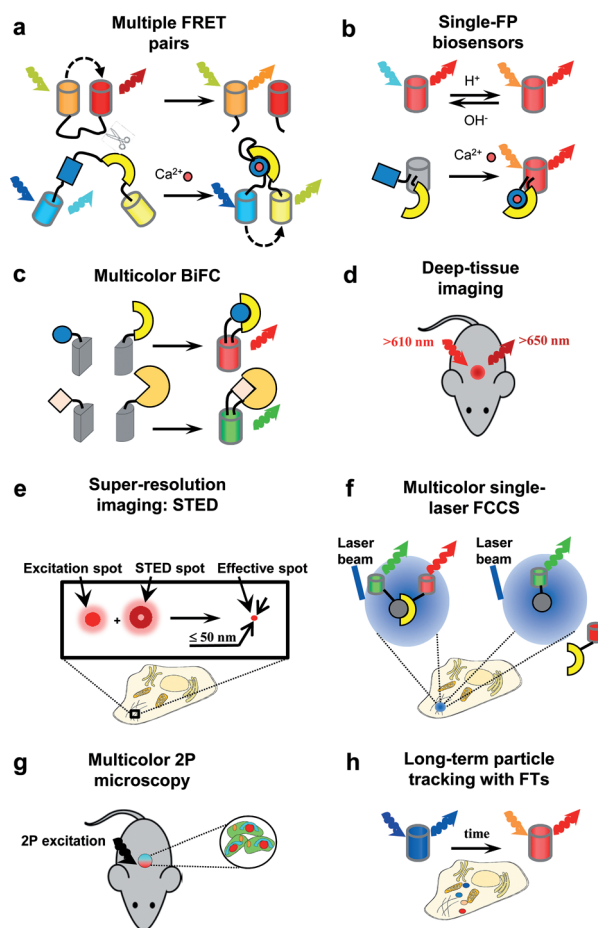

Figure 1. Applications of permanently fluorescent RFPs of different phenotypes. Cylinders represent FPs, which are colored corresponding to their emission spectral range. Colored arrows denote the respective excitation or emission light. a) Multiple FRET pairs. Several spectrally distinguishable FRET-biosensors may be used for simultaneous imaging of multiple FRET pairs. A combined orange FP–far-red FP caspase biosensor (top panel) and CFP–YFP calcium biosensor (bottom panel) are shown as examples; b) Single-FP biosensors. A shift in excitation/emission maxima (top panel, pH sensor) or a change in intensity (bottom panel, calcium sensor) under specific stimuli is the readout of these biosensors; c) Multicolor BiFC. Several independent pairs of interacting proteins may be identified; d) Deep-tissue imaging. This application requires far-red FPs exhibiting excitation and emission maxima within the NIRW (650–690 nm) to obtain the highest light transmission and the lowest autofluorescence; e) Super-resolution imaging: Most commercially available STED microscopes use a 638 nm excitation beam (red circle), which is superimposed with a doughnut-shaped STED beam (750 nm). The STED beam instantly quenches excited FPs at the periphery of the excitation area, thus confining the fluorescence emission to a spot of only a few tens of nanometers (red dot). To date, using FPs a resolution of 50 nm can be achieved;[29] f) Multicolor single-laser FCCS. A single excitation wavelength is used for a set of LSSFPs fluorescing at different wavelengths; g) Multicolor two-photon microscopy. With this technique, a subcellular resolution in deep tissues can be achieved with 2P single wavelength excitation of a set of LSSFPs fluorescing at different wavelengths; h) Long-term particle tracking with FTs. A slow change of FT color allows prolonged tracking of the particle inside the cell.

Light sheet microscopy techniques include selective-plane illumination microscopy (SPIM),[21] orthogonal-plane fluo-

Table 1: Spectral and biochemical properties of modern RFPs.

Protein	λmax(abs) [nm]	λmax(em) [nm]	ε [M⁻¹ cm⁻¹]	Φ	Brightness[a] [mM⁻¹ cm⁻¹]	pKa[b]	Photostability [s][c]	Oligomeric state[d]	Additional property	Ref.
FPs with autocatalytic formation of chromophore										
Conventional FPs									Maturation at 37°C $t_{1/2}$ [h]	
mOrange2	549	565	58 000	0.60	35	6.5	228	M	4.5	[6]
mKOκ	551	563	105 000	0.61	64	4.2	n.d.[e]	M	1.8	[10]
TagRFP-T	555	584	81 000	0.41	33	4.6	337	M	1.7	[6]
mRuby	558	605	112 000	0.35	39	5.0	127[f]	M	2.8	[11]
mCherry	587	610	72 000	0.22	16	<4.5	96	M	0.25	[7]
tdTomato	554	581	138 000	0.69	95	4.7	98	TD	1	[7]
Far-red FPs										
mKate2	588	633	62 500	0.40	25	5.4	93[f]	M	<0.33	[48]
Katushka	588	635	65 000	0.34	22	n.d.[e]	n.d.[e]	D	0.33	[38]
mNeptune	600	650	67 000	0.20	13	5.4	226[f] 48[g] 34.5[f]	M	0.6	[31] [32] [33]
TagRFP657	611	657	34 000	0.10	3.4	5.0	205[g]	M	2.1	[32]
eqFP650	592	650	65 000	0.24	16	5.7	30[f]	D	Fast	[33]
eqFP670	605	670	70 000	0.06	4.2	4.5	206[f]	D	Fast	[33]
E2-Crimson	611 605	646 646	126 000 58 500	0.23 0.12	29 7.1	4.5	105[g] 3[f]	T	0.4	[4] [33]
LSSFPs										
LSSmOrange	437	572	52 000	0.45	23.4	5.7	21[h]	M	2.3	[43]
mKeima	440	620	14 400	0.24	3.5	6.5	19	M-D	4.5	[44]
LSSmKate1	463	624	31 200	0.08	2.5	3.2	60[h]	M	1.7	[45]
LSSmKate2	460	605	26 000	0.17	4.4	2.7	44[h]	M	2.5	[45]
FTs									Characteristic times [h][i]	
Slow-FT	402 583	465 604	33 400 84 200	0.35 0.05	12 4	2.6 4.6	n.d.[e] n.d.[e]	M	9.8 28	[49]
Medium-FT	401 579	464 600	44 800 73 100	0.41 0.08	18 6	2.7 4.7	n.d.[e] n.d.[e]	M	1.2 3.9	[49]
Fast-FT	403 583	466 606	49 700 75 300	0.30 0.09	15 7	2.8 4.1	n.d.[e] n.d.[e]	M	0.25 7.1	[49]
mK-GO	500 548	509 561	35 900 42 000	n.d.[e] n.d.[e]	n.d.[e] n.d.[e]	6.0 4.8	n.d.[e] n.d.[e]	M	6	[50]

Protein	λmax(abs) [nm]	λmax(em) [nm]	ε [M⁻¹ cm⁻¹]	Φ	Brightness[a] [mM⁻¹ cm⁻¹]	pKa[b]	Photostability [s][c]	Contrast ratio[j]	Photoactivation/photo switching light [nm]	
Irreversibly photoactivatable FPs										
PAmCherry1	(404) 564	n.d.[e] 595	6500 18 000	n.d.[e] 0.46	n.d.[e] 8.3	n.d.[e] 6.3	n.d.[e] 91[f]	4000	405	[51]
PATagRFP	(278) 562	n.d.[e] 595	n.d.[e] 66 000	n.d.[e] 0.38	n.d.[e] 25	n.d.[e] 5.3	n.d.[e] 161[f]	540	405	[52]
PAmKate	(442) 586	n.d.[e] 628	n.d.[e] 25 000	n.d.[e] 0.18	n.d.[e] 4.5	n.d.[e] 5.6	n.d.[e] 433[f]	100	405	[53]
Dendra2	490 553	507 573	45 000 35 000	0.50 0.55	23 19	6.6 6.9	45 378	300	405/488	[54]
mEos2	506 573	519 584	56 000 46 000	0.84 0.66	47 30	5.6 6.4	42 323	n.d.[e]	405	[55]
mKikGR	505 580	515 591	49 000 28 000	0.69 0.63	34 18	6.6 5.2	14 21	400	405	[56]
mClavGR2	488 566	504 583	19 000 32 000	0.77 0.53	15 17	8.0 7.3	17 175	n.d.[e]	405	[67]
mIrisFP	(386) 486 (446) 546	n.d.[e] 516 n.d.[e] 578	12 000 47 000 21 000 33 000	n.d.[e] 0.54 n.d.[e] 0.59	n.d.[e] 25 n.d.[e] 19	5.4 7.6	n.d.[e] n.d.[e]	n.d.[e] 405	473 405 561 473	[57]
NijiFP	(ca. 375) 469 (ca. 440) 526	n.d.[e] 507 n.d.[e] 569	12 000 41 100 21 000 42 000	n.d.[e] 0.64 n.d.[e] 0.65	n.d.[e] 26 n.d.[e] 27	7.0 7.3	n.d.[e] n.d.[e]	n.d.[e] 405	488 405 561 440	[58]
PSmOrange	548 636	565 662	113 300 32 700	0.51 0.28	58 9.2	6.2 5.6	489[k] 1580[k]	560	480-540	[37]
Reversibly photoswitchable FPs										
rsCherry	572 572	610 610	81 000 80 000	(0.009) (0.02)	0.7 1.6	n.d.[e] (6.0)	n.d.[e] n.d.[e]	3(20)	450 550	[51] ([59])
rsCherryRev	572 572	608 608	41 800 42 300	0.0017 0.0051	0.07 0.22	n.d.[e] (5.5)	n.d.[e] n.d.[e]	3(7)	550 450	[60] ([59])
rsTagRFP	440 567	585 585	15 300 36 800	0.0013 0.11	0.02 4	n.d.[e] 6.6	n.d.[e] n.d.[e]	20	570 440	[60]

[a] Brightness determined as the product of extinction coefficient ε and quantum yield Φ. [b] pKa is the pH value at which fluorescence is half-maximal. [c] A time required for photobleaching of 50% of fluorescence signal. To account for different efficiencies of FP excitation and microscope setups, the values are normalized to spectral output of the lamp, transmission profiles of the filters, and the dichroic mirror used in the photobleaching experiment, and to the absorbance spectra of FP. [d] M, D, TD, and T indicate monomer, dimer, tandem dimer, and tetramer, respectively. [e] n.d. = not determined. [f] Determined relative to mCherry.[7] [g] Determined relative to mKate2.[48] [h] Determined relative to mKeima.[44] [i] The occurrence of the maximal blue fluorescence intensity and half-maximal red (or orange) fluorescence intensity were considered as characteristic times of FTs. [j] The ratio of fluorescence intensity after photoconversion to fluorescence intensity before photoconversion. [k] Determined relative to mOrange2.[6]

Table 2: RFP phenotypes and properties required for specific applications.

Application	RFP phenotype	Major required properties
FRET imaging	Conventional RFPs, far-red FPs, LSSFPs	Brightness, photostability, pH stability, fast and complete maturation
Imaging of single-FP biosensors	cpFPs, LSSFPs	Reversible change in spectra with specific stimuli, brightness, photostability, efficient maturation
Multicolor BiFC	Split RFPs	Brightness, photostability, pH stability, fast and efficient complementation
Deep tissue imaging	Far-red FPs	Excitation/emission near or in NIRW, brightness, low cytotoxicity
STED	Far-red FPs	Photostability, brightness, monomeric state
FCCS	LSSFPs	Brightness, photostability, fast and complete maturation, monomeric state
Two-photon microscopy	LSSFPs	Two-photon brightness, two-photon photostability
Long-term tracking with FTs	FTs	Brightness, photostability, efficient maturation of both forms, high contrast between fluorescence of two forms
Time-lapse imaging with selective photolabeling	PAFPs, PSFPs	Photoactivation contrast, wavelength of photoactivation light, photostability of photoconverted form, low phototoxicity
Long-term intravital imaging with photolabeling	PAFPs, PSFPs	Far-red shifted fluorescence, low cytotoxicity, longer wavelength of photoswitching light, photostability, intracellular lifetime
PALM based techniques	PAFPs, PSFPs, rsFPs	Photoactivation contrast, single-molecule brightness (photon output), fatigue resistance (for rsFPs), monomeric state
Photochromic FRET	rsFPs	Shift in absorbance spectra of an acceptor upon photoswitching, high extinction coefficients, photostability, complete maturation
RESOLFT	rsFPs	Brightness, fatigue resistance, photostability, photoswitching rate, photoconversion contrast, monomeric state

rescence optical sectioning (OPFOS),[22] highly inclined and laminated optical sheet (HILO)[23] microscopy, and their derivatives. In SPIM, a sample is illuminated from the side in a well-defined volume around the focal plane of the detection optics (reviewed in Ref. [24]). The illumination plane and the detection paths are perpendicular to each other. The major advantage of the SPIM approach is the fast image acquisition. Application of RFPs to SPIM and other light-sheet fluorescence microscopy approaches has been limited to date.

2P microscopy has a superior performance in deep-tissue imaging because of its reduced out-of-focus fluorescence and light scattering, combined with a better penetration of infrared light.[26] In addition, 2P imaging reduces the overall photobleaching in thick samples by limiting it to the focal plane.[25] However, since 2P femtosecond pulsed excitation intensities result in up to around 10-fold faster photobleaching than using standard one-photon (1P) excitation,[26] the use of 2P imaging for thin samples is suboptimal.

2P imaging of conventional orange and red FPs was limited by the low power output above 1000 nm of standard tunable mode-locked Ti-Sapphire lasers, which are used for commercial 2P microscopes. To compensate for the substantial decrease in brightness above 1000 nm, optical parametric oscillators (OPO) were employed. The OPO femtosecond pulsed 2P sources provide light output from 1000 nm to 1600 nm, with the maximal output power at around 1200 nm. Despite the commercial availability of stand-alone OPO systems, OPO light sources on biological microscopes have only recently become available. In addition, custom-built two-laser 2P microscopes capable of exciting fluorophores in the ranges 750–1040 nm and 1100–1600 nm have been described.[27] Wider use of the 2P OPO sources should extend the applicability of RFPs in 2P imaging.

It has been shown that the 1P characteristics of FPs do not allow their 2P properties to be predicted unambiguously.[28] Unlike a 1P absorption cross-section (i.e., extinction coefficient), a 2P absorption cross-section is sensitive to an electric field around the chromophore in a FP molecule and is influenced by charged amino acids and hydrogen-bonding networks in the chromophore microenvironment. It is also not possible to precisely predict an optimal 2P excitation wavelength from the 1P excitation spectrum. Furthermore, photobleaching pathways differ at 1P and 2P light irradiation.[26] Therefore, RFPs specifically optimized for 2P excitation are required (Table 2).

3. Far-Red FPs

Engineering far-red shifted bright FPs is a rapidly developing area. The far-red FPs are superior to FPs of other colors for tissue and whole-body imaging because mammalian tissue is more transparent to far-red light as a result of the high absorbance of hemoglobin below 650 nm.[30] To satisfy the needs of deep-tissue imaging, a number of novel far-red FPs have been developed recently. The most far-red shifted FPs are monomeric mNeptune[31] and TagRFP657,[32] dimeric eqFP650,[33] eqFP670,[33] and tetrameric E2-Crimson[4] (Table 1). E2-Crimson, eqFP650, and eqFP670 were specifically optimized for low cytotoxicity.

Moreover, several near-infrared FPs, such as IFP1.4[34] and iRFP,[35] have been developed recently on the basis of bacterial phytochromes. Fluorescence of these proteins is dependent on an exogenous tetrapyrrole chromophore, called biliverdin, which is abundant in mammalian cells. Bacterial phytochromes present promising templates for engineering future far-red and infra-red FPs. Currently available FPs in this range are not as bright as organic dyes. The brightest far-red E2-Crimson is 3-times less bright than Alexa647.[1b] The enhanced genetically encoded far-red probes are in a high demand.

3.1. Far-Red FPs in Whole-Body Imaging

An optimal probe for whole-body imaging should have excitation and emission spectra within an 650–950 nm "near-infrared optical window" (NIRW) in which mammalian tissues have the lowest absorbance by hemoglobin, melanin, and water[30] (Figure 1d, Table 2). The tissue absorbance in NIRW drops so significantly that even dim far-red FPs perform substantially better than bright-green FPs.[36] None of conventional far-red FPs developed so far has excitation maxima within the NIRW. The practical usefulness of FPs for deep tissue imaging can be evaluated by determining their apparent brightness under excitation wavelengths near to the NIRW in live animals. Recent studies compared far-red FPs using various approaches, such as injecting samples of purified FPs[36,37] or mammalian cells expressing FPs into animals,[33] directly expressing FPs in *Xenopus* embryos,[38] or in transgenic mice.[39] mKate2, mNeptune, eqFP650, and Katushka outperformed other red and far-red FPs. It is important that far-red FPs applied to live imaging have low cytotoxicity.

3.2. Far-Red FPs in Super-Resolution Imaging

Far-red FPs have also found their application in super-resolution imaging. Red-shifted excitation of E2-Crimson[4] and TagRFP657[32] was utilized in a super-resolution stimulated emission depletion (STED)[40] microscopy study using commercial STED microscopes equipped with 635–640 nm excitation lasers (Figure 1e). Because E2-Crimson is tetrameric it can be mainly used to label whole cells and lumenal spaces of organelles. TagRFP657 is a monomer, and was fused to individual cellular proteins to obtain STED images.[32] The major requirement for FP for efficient STED imaging is its high photostability (Tables 2 and 3).

4. RFPs with a Large Stokes Shift

A large Stokes shift (LSS), that is, a difference between excitation and emission maxima larger than 100 nm, is a distinctive feature of a subclass of FPs, called LSSFPs. LSSFPs provide spectrally resolvable colors for multicolor imaging applications. In addition to green[41] and yellow[42] LSSFPs there are orange LSSmOrange[43] and three red LSSFPs, mKeima,[44] LSSmKate1, and LSSmKate2[45] (Table 1). All red-shifted LSSFPs absorb at 440–460 nm and fluoresce in red part of the spectrum. LSSmOrange exhibits the highest brightness among red-shifted LSSFPs. LSSmKate2 outperforms mKeima in terms of pH-stability, photostability, and brightness. It also lacks an additional excitation peak in the yellow spectral region. Evaluation of LSSmKate2 in stably expressing mammalian cells showed its low cytotoxicity.[45]

4.1. LSSFPs in FCCS: Two-photon and FRET Applications

Spectral properties of LSSFPs are advantageous for multicolor applications using a single excitation wavelength (Table 2). Fluorescence cross-correlation spectroscopy (FCCS) is a variation of fluorescence correlation spectroscopy (FCS), which is optimized to study the interaction between proteins of relatively similar molecular weights. In dual-color FCCS, the degree of cross-correlation between two signals correlates with the percentage of interacting pairs. In contrast to FRET, FCCS does not depend on close proximity and a favorable orientation between FPs.[46] Single-laser dual-color FCCS is advantageous over a two-laser setup because it does not require the precise alignment of two lasers to the same confocal spot. The red LSSFP, mKeima was efficiently excited together with CFP by the same laser, resulting in dual-color FCCS[44] (Figure 1f). This strategy has been expanded to achieve four-color FCCS by using blue FP, green LSSFP, LSSmOrange, and LSSmKate1.[43]

A relatively slow speed of wavelength tuning in commercial 2P microscopes limits simultaneous imaging of fast dynamic events using multicolor probes. Use of red LSSFPs together with cyan FPs excited with a single 2P excitation wavelength has allowed real-time dual-color 2P imaging[45,47] (Figure 1g).

Red LSSFPs are attractive probes for FRET applications. They are putative donors for far-red FPs and potential acceptors for blue FPs. A large separation between the excitation of a red LSSFP donor and the emission of a red LSSFP acceptor in the spectra of the corresponding FRET partners should result in a low-background and high-sensitivity FRET assay. The LSSFP-based FRET pairs could also be combined with other FRET pairs (Figure 1a). Recently, a LSSmOrange–mKate2 FRET pair was used with a CFP–YFP FRET biosensor to simultaneously image two processes in a single cell.[43]

4.2. LSSFPs in Single-FP Biosensors

Single-FP ratiometric biosensors (Figure 1b) could be developed from LSSFP variants that can be switched between two states, which have either a large Stokes shift or a regular Stokes shift fluorescence, upon a specific stimuli. The corresponding chromophore transformation between a neutral state and an anionic state (see Section 8) provides the basis to design such biosensors. A pH-biosensor, pHRed, with emission at 610 nm was developed from mKeima.[61] Its readout is a ratiometric change in the excitation maxima at 440 nm and 585 nm. Ratiometric sensors are preferable over other types because they are not influenced by artifacts caused by variable protein concentration, cell thickness, cell movement, and excitation intensity. Moreover, the pHRed biosensor allowed dual-color imaging in combination with a green ATP sensor, called Perceval.[61]

5. Fluorescent Timers

A fluorescent timer (FT) protein changes its fluorescent color over time. This phenomenon is based on a slow chromophore formation process with intermediate and final chromophore forms fluorescing in different spectral ranges. The predictable time course of the color changes allows quantitative analysis of temporal and spatial events in vivo (Figure 1h). In contrast to photoactivatable FPs described in Section 6 and suitable to study fast intracellular dynamics, FTs are typically applied to investigate relatively slow events.

There are two types of FTs. FTs of the first type, mCherry-derived monomeric fast (Fast-FT), medium (Medium-FT), and slow (Slow-FT) FTs (Table 1), change their fluorescence from blue to red over time.[49] The blue and red forms of FTs are bright and pH-stable, and the conversion of the blue form into the red form is complete. However, a noticeable blue-to-red photoconversion under irradiation with intense violet light complicates their use (Table 2). Another type of FT, monomeric Kusabira Green Orange (mK-GO) (Table 1) changes its color from green to orange with time.[50] In contrast to mCherry-derived FTs, two forms of mK-GO mature independently. The green form does not disappear after maturation of the orange form. The orange-to-green ratio changes from about 0.1 initially to 0.7 after complete maturation. Although the light sensitivity of mK-GO was not examined, the independent maturation of both forms should prevent green to orange photoconversion.

Monomeric FTs can be used to estimate the age of proteins tagged with FT. It has been possible with Medium-FT[49] and mK-GO[50] to determine the age of compartments that took part in autophagy and endocytosis.

6. Photoactivatable RFPs

FPs with fluorescent properties regulated by light are suitable for use in various selective photolabeling techniques, from particle tracking to super-resolution imaging. This group of FPs is termed photoactivatable FPs (PAFPs). Important characteristics of PAFPs are the photoactivation contrast and the brightness of both initial and photoactivated forms. The photoactivation contrast is the ratio of fluorescence intensity after photoactivation to the fluorescence intensity before photoactivation. In the case of photoswitchable FPs (PSFPs), it is defined as the intensity ratio between two fluorescent forms, before and after photoconversion.[62] A higher contrast results in a greater signal-to-background ratio. Another parameter to consider is the intensity of light required for photoactivation: it should not be so high that it is harmful to a cell, or so low that spontaneous photoactivation would occur.

Currently there are three types of irreversible red PAFPs: dark-to-red photoactivatable PAmCherry-like RFPs, green-to-red photoswitchable Kaede-like RFPs, and orange-to-far-red photoswitchable FPs represented by the recently developed PSmOrange.

Dark-to-red PAFPs, such as PAmCherry[51] and PATagRFP[52] (Table 1), undergo activation from a dark to red fluorescent form on irradiation with 405 nm violet light. PATagRFP outperforms PAmCherry in brightness and photostability. The recently designed dark-to-far-red PAmKate extends the spectral range beyond that available with the other two PAFPs.[53]

PSFPs of the Kaede-like type are converted from a green form to a red fluorescent form with violet light. Monomeric Dendra2,[54] mEos2,[55] and mKikGR[56a] are currently among the best available PSFPs of this group (Table 1). Recently, a rational design was applied to conventional monomeric cyan FP resulting in a green-to-red mClavGR2 PSFP.[56b]

Based on EosFP[63] and Dendra2 variants, several FPs with a complex phenotype, which have properties of both irreversible and reversible PSFPs, were developed. First, similarly to Kaede-like PSFPs, an irreversible photoswitching of IrisFP,[64] its monomeric variant mIrisFP,[57] and NijiFP[58] to green and red forms occurs simultaneously on irradiation with violet light. Subsequent irradiation of the green forms of these FPs with 488 nm and low-intensity 405 nm lasers reversibly switches their green chromophore off and on, respectively. Irradiation of the red forms with 532 nm light drives the red chromophores into the off state whereas irradiation with 440 nm light switches them on (Table 1).

Recently reported PSmOrange[37] is orange in its initial state and becomes far-red after irradiation with blue–green light (Table 1). The red-shifted emission of both forms, compared to green-to-red PSFPs, and the longer wavelength of the photoswitching light used are advantageous for its live-cell applications (Table 2).

6.1. PAFPs as Photolabels for Long-Term Imaging

PAFPs can serve as selective photolabels for a protein of interest, a specific organelle, or a cell. Photomarking a protein fused to PAFPs is used to study protein dynamics and turnover. Organelle photolabeling allows the monitoring of fission and fusion events. Cell tracking is applied to study development, carcinogenesis, and inflammation.[87] Specific characteristics that make PAFPs suitable for long-term tracking in vivo include their photoactivation contrast, wavelength of photoactivation light, photostability of the activated form, phototoxicity, and the turnover rate of the PAFP or its fusion construct (Table 2). The last three parameters limit the time during which the photolabeled object can be followed.

It is useful when PAFPs in the initial state can be imaged with light that does not cause photoactivation. Therefore Kaede-like proteins, such as mKikGR,[56a] mEos2,[55] Dendra2,[54] and their derivatives are currently the preferred monomeric photolabels for various types of tracking experiments. Dendra2 is of special interest because it can be photoconverted with blue light that is less harmful for cells than violet light.[54] It was applied to monitor the metastatic behavior of individual tumor cells in living mice[87b] and to image actin polymerization in invasive structures of murine macrophages and adenocarcinoma cells.[88] New possibilities for particle tracking have been created with the development of PSmOrange.[37] This PSFP is spectrally resolvable with cyan-to-green PSCFP2 protein[54] and, thus, can be used for

simultaneous tracking four different cellular populations. The orange and far-red colors of PSmOrange can be resolved with common mCherry. Because it requires blue-green light for photoconversion, which is absorbed by tissues ten-fold less than violet light, PSmOrange can be photoconverted inside a living mouse[37] (Figure 2 a).

New applications may arise from the use of PAFPs in FRET imaging. A simple approach can be based on the photoactivation of a specific PAFP in one cellular compartment and the subsequent monitoring of FRET between the PAFP donor and a conventional RFP acceptor in a different cellular region. Another potential approach implies a FRET-facilitated photoswitching in which PAFP photoconversion is caused by FRET from a FP donor. This approach could be applied to map the fate of protein interactions in a cell.

6.2. PAFPs in Super-Resolution Imaging

The PAFP phenotype is crucial for photoactivated localization microscopy (PALM)[65] and similar fluorescence PALM (FPALM)[75] super-resolution methods (Table 3, Figure 2 b). PALM relies on single-molecule imaging. The single-molecule brightness (defined as the number of emitted photons) and the contrast between the background and photoactivated photon outputs are the critical FP properties for this group of techniques (Tables 2 and 3). Since in PALM approaches a higher contrast results in a higher spatial resolution, red-shifted FPs whose imaging is accompanied by a lower autofluorescent background are the preferred PALM probes.

Dark-to-red PAFPs PAmCherry[51] and PATagRFP[52] are valuable tools for two-color PALM. In contrast to green-to-red Kaede-like PSFPs, these proteins lack green fluorescence. This property allows their use simultaneously with green PAFPs. Two-color PALM with PAmCherry and PAGFP has been demonstrated to image clusters of transferrin receptors and clathrin molecules at 25 nm resolution.[51] PATagRFP together with PAGFP was applied to two-color single-particle tracking PALM (sptPALM) in live cells.[52] The sptPALM approach is useful for studying the stoichiometry of two colocalized or interacting proteins at a single-molecule level. FPALM imaging of three PAFPs simultaneously in both live and fixed cells was achieved with dark-to-far-red PAmKate together with PAmCherry1 and Dendra2.[53] PSmOrange was also utilized in PALM imaging that, for the first time, used activation light at 488 nm.[37]

It has been shown that PAmCherry photoactivation is also possible with a 2P irradiation. This property was utilized to image intracellular structures at high resolution (< 50 nm lateral and < 100 nm axial resolution) at depths of approximately 8 µm using 3D PALM.[80] Furthermore, PAmCherry was applied to a combination of PALM and SPIM techniques in 3D super-resolution imaging of a live cell.[89]

Among Kaede-like PSFPs, the favorite probes for PALM are tdEosFP, mEos2, and Dendra2. tdEosFP[90] has a large photoswitching contrast and high photon output. This protein demonstrated good performance in both 2D[91] and 3D[92] PALM approaches. The use of tdEosFP in 3D interferometric PALM (iPALM), which combines PALM with simultaneous multi-phase interferometry of photons from each fluorescent molecule, allowed the mapping of the nanoscale protein organization in focal adhesions.[92] Since smaller probes are preferred as fusion tags, to give a more accurate localization of a fusion protein, monomeric mEos2 is a good alternative to the twice as large tandem dimeric tdEosFP.[55,93] Monomeric Dendra2 was applied to polarization FPALM to determine the orientations of single molecules in cellular structures.[82] mIrisFP and NijiFP can be reversibly and irreversibly photoswitched and were used in super-resolution imaging coupled with pulse-chase selective photolabeling.[57,58]
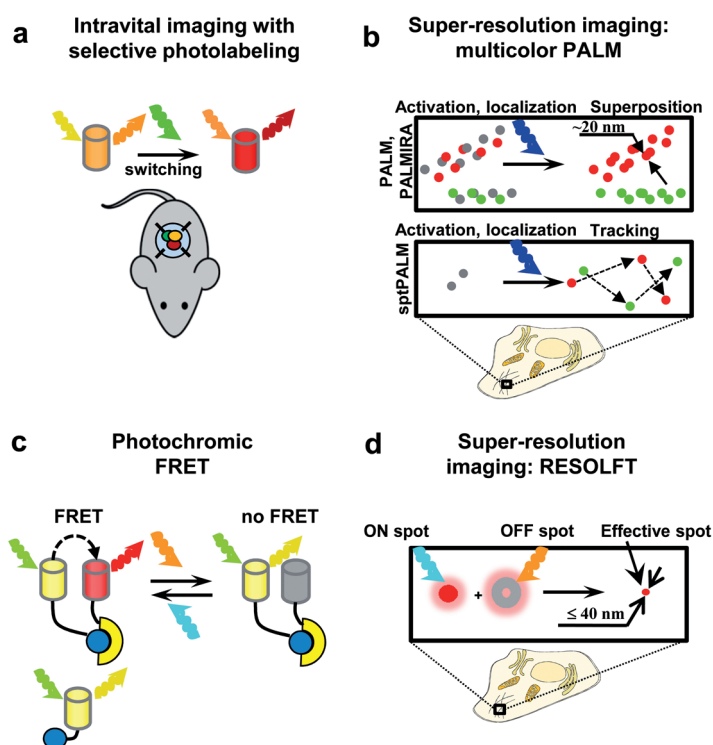

Figure 2. Applications of irreversibly and reversibly photoswitchable RFPs. Cylinders represent FPs, which are colored corresponding to their emission spectral range. Colored arrows denote the excitation, emission, and photoactivation light. a) Intravital imaging with selective photolabeling. PSFPs may be photoswitched inside an animal, and the photolabeled cells can be tracked; b) Super-resolution imaging with PALM-based techniques: multicolor PALM, PALMIRA (with rsFPs), and sptPALM. PALM microscopy is based on the accurate localization (up to ca. 20 nm)[65] of individual PAFP molecules (colored dots). The imaging cycle includes the stochastic photoactivation of the PAFPs molecules, imaging, and subsequent photobleaching of the photoactivated molecules. The cycle is repeated many times to reconstruct a super-resolution image. sptPALM allows tracking of localized single molecules in live cells; c) Photochromic FRET. rsFPs that change their absorbance upon photoswitching are used in photochromic FRET. The process of FRET occurs when rsFP is in the ON state, and does not occur when rsFP is in the OFF state. Thus, pcFRET allows a control image of the same sample to obtained without FRET by temporarily switching it the FRET OFF; d) Super-resolution imaging: RESOLFT microscopy utilizes an ON beam (blue arrow) and a superimposed doughnut-shaped OFF beam (yellow arrow) to confine a diffraction-limited spot of switched ON rsFP molecules to a subdiffraction-sized spot (red dot). The resolution achieved to date using FPs is 40 nm.[66]

Table 3: Super-resolution fluorescence microscopy techniques with FPs.

Far-field super-resolution approaches are based on the ability to switch fluorescent probes, such as FPs and organic dyes, on and off by utilizing different transitions in a fluorescent molecule (reviewed in Ref. [67]). These techniques can be divided into two major groups: the first based on a patterned illumination and the second based on a molecular localization. The first group relies on a nonlinear imaging of molecules in ensemble, whereas the second one is based on an optical detection of single molecules combined with a subsequent reconstruction of their coordinates.

Techniques based on imaging in ensemble mode

These fluorescence microscopy techniques include stimulated emission depletion (STED),[68] ground-state depletion (GSD),[69] saturated structured illumination microscopy (SSIM),[67b] and reversible saturatable optical (fluorescence) transition (RESOLFT).[70] STED utilizes a transition between the fluorescent singlet state and the ground state of a probe. The same states are used in SSIM, whereas fluorescent singlet and long-lived dark triplet states are utilized in GSD. RESOLFT is based on switching between the metastable fluorescent and dark states of reversibly switchable probes.
In STED, the specimen is illuminated by two synchronized ultrafast pulsed light beams: the excitation laser pulse and the co-linear depletion laser pulse. The resulting doughnut-shaped depletion around the diffraction-limited excitation spot produces a sharpened effective fluorescent spot with an increase in the resolution up to tens of nanometers in the lateral direction. A super-resolution image is built by scanning these two beams across the sample. For the depletion of the excited state of FPs, STED requires extremely high intensities of light ($10\ MW\,cm^{-2}$), which is a limitation for live-cell imaging.[67a, 71] Because the same spot is scanned several times to reconstitute an image, the most important characteristic of a fluorescent probe is its photostability. Probes that are bright and completely un-excitable by the wavelength of the depletion laser are also preferable. A resolution of around 50 nm has been reported for STED with FPs.[29]
GSD requires the lower light intensities (ca. $10\ kW\,cm^{-2}$)[69] than STED. In SSIM, the illumination pattern is formed by the interference of two collimated beams, scanned across the sample.[72] Moderate illumination intensities in SSIM (ca. $100\ W\,cm^{-2}$) allow live-cell imaging.
Since RESOLFT utilizes cycling between two metastable states of a probe it requires low intensities of light, such as 1–$10\ W\,cm^{-2}$.[67a] RESOLFT can be applied to live-cell super-resolution microscopy.[73] Typically around 1000 switching cycles are required to achieve a 10-fold better resolution.[67b] Therefore, the crucial probe property is fatigue resistance.[74] Recently a rsFP with high photostability has been applied to RESOLFT resulting in a resolution of 40 nm in live cells.[66]

Techniques based on single-molecule imaging

These techniques include photoactivated localization microscopy (PALM),[65] fluorescent PALM (FPALM),[75] stochastic optical reconstitution microscopy (STORM),[76] direct STORM (dSTORM),[77] ground-state depletion microscopy (GSDIM),[78] bleaching-blinking assisted localization microscopy (BaLM),[79] and various related approaches, such as a single-particle tracking PALM (sptPALM),[52] 3D-PALM,[80] 3D iPALM,[81] PALM with independently running acquisition (PALMIRA),[59] polarization FPALM,[82] PALM with stroboscopic illumination (S-PALM),[83] live-cell PALM,[84] and multicolor PALM,[51] among others. All of them utilize switching between the fluorescent state and the dark state of a fluorescent probe, except GSDIM, which uses a transition between the fluorescent singlet state and the long-lived dark triplet states.
In PALM, a small fraction of individual PAFP molecules are stochastically photoactivated with a low light intensity, and then imaged and photobleached. This process is repeated many times for recording images of distantly located subsets of molecules. Then the stack of images is processed to localize single molecules by finding the centroid positions in their point spread functions. The final super-resolution image is reconstructed by merging of all the localized single-molecule positions. Single-molecule detection is subject to considerable random noise. To reduce it, initially PALM was demonstrated in a combination with a total internal reflection (TIRF) imaging mode[65] while a similar FPALM method was implemented in a wide-field format.[75] A lateral resolution of 20 nm has been achieved using PALM with PAFPs.[65]
STORM and its derivatives are based on the same principles as PALM but historically utilize photoconvertible organic dyes. Both PALM and STORM require much lower light intensities for photoactivation and imaging (1–$100\ W\,cm^{-2}$) than STED.[65, 85] In PALM- and STORM-based approaches a precision of single-molecule localization depends on the number of emitted photons by a photoactivated molecule (photon output). The higher single-molecule brightness results in better resolution. Besides photon output, high photoactivation contrast of PAFPs is advantageous to achieve a better signal-to-noise ratio and, subsequently, higher resolution.
Whereas PALM typically uses PAFPs, its derivative, PALMIRA, utilizes rsFPs. PALMIRA improves the rate at which data are acquired by a factor of 100.[86] A resolution of around 45 nm was achieved with PALMIRA using rsFPs.[73] PALM has been also extended for a use with conventional fluorescent probes in BaLM. BaLM imaging is based on an intrinsic ON–OFF blinking behavior of fluorescent chromophores. BaLM has provided a lateral resolution of around 50 nm.[79]

7. Reversibly Photoswitchable RFPs

Reversibly photoswitchable FPs (rsFPs) can be repeatedly photoswitched between fluorescent and non-fluorescent states. This property allows new imaging applications. Recently developed red rsFPs include rsCherry,[59] rsCherryRev,[59] and rsTagRFP[60] (Table 1). Irradiation of rsTagRFP with 550–570 nm light switches off a red fluorescent state, which absorbs at 567 nm, into a dark state absorbing at 440 nm. Irradiation with 430–450 nm light switches the dark state back to the fluorescent state. rsCherry and rsCherryRev are red rsFPs that can be switched reversibly between states by irradiating alternately with 550–560 nm and 440–450 nm light.[59] rsTagRFP exhibits higher brightness and 6-times

higher photoswitching contrast than rsCherry and rsCherryRev.

The difference in the absorbance spectra of the rsTagRFP's fluorescent and dark states enabled its use as an acceptor in photochromic FRET (pcFRET) with yellow FPs as the donors[60, 94] (Figure 2c, Table 2). pcFRET is a light-induced reversible FRET switching that is achieved by changing the absorbance of a FRET acceptor. pcFRET facilitates detection of protein–protein interactions and provides an internal control for FRET.

A reversibly switchable phenotype may provide advantages for super-resolution techniques. However, in practice, super-resolution imaging using rsFPs has been limited by the lack of "fatigue resistant" FPs, which could be reversibly photoswitched a hundred times without photobleaching

(Table 3). In addition, brightness and contrast of the best available red rsFPs are not as good as those of red PAFPs and PSFPs (Table 1). To date, three types of super-resolution techniques based on rsFPs have been reported, these are reversible saturable optical (fluorescence) transitions (RESOLFT)[67a] (Figure 2 d), PALM with independently running acquisition (PALMIRA),[59] and PALM with two-color stroboscopic illumination (S-PALM) microscopy.[83] Red rsFPs have been applied in RESOLFT to image bacteria using tetrameric asFP595 rsFP.[95] A lateral resolution of 50–100 nm was achieved. Use of rsCherryRev for time-lapse live cell PALMIRA imaging of the endoplasmic reticulum provided around 75 nm resolution.[59] Future fatigue-resistant red rsFPs should improve the RESOLFT and PALMIRA performance and enable these techniques to be used widely to study intracellular processes with super-resolution accuracy (see Table 3).

8. Chromophore Chemistry

Rapidly developing imaging applications require an improvement of RFP probes. The rational design of new RFPs is based on knowledge of the principles of chromophore formation and functioning. A number of diverse approaches including crystallography,[2f,g,96] mutagenesis, isotope studies,[2i,97] steady-state and time-resolved spectroscopy,[97,98] mass-spectrometry,[37,96a] electronic structure calculations,[99] and synthesis of model chromophores,[100] have been applied to reveal transformations of red chromophores. There is now sufficient information available to develop a rational strategy in RFP design.

In RFPs, a chromophore-forming tripeptide consists of invariant Tyr66 and Gly67 amino acid residues and a variable residue 65 (the numbering follows that for the *Aequorea victoria* GFP). A core 4-(*p*-hydroxybenzylidene)-5-imidazolone structure is common to all red chromophores, while

modifications of the protein backbone at position 65 vary, resulting in a range of known red-shifted chromophores (Figure 3).

There are two major types of red chromophores: DsRed-like[101] and Kaede-like[2c] (Figure 3). The DsRed-like chromophore is formed as a result of either autocatalytic or photoinduced transformations of the X65-Tyr66-Gly67 tripeptide whereas the Kaede-like red chromophore is characterized by the His65-Tyr66-Gly67 chromophore tripeptide and is only generated photochemically.
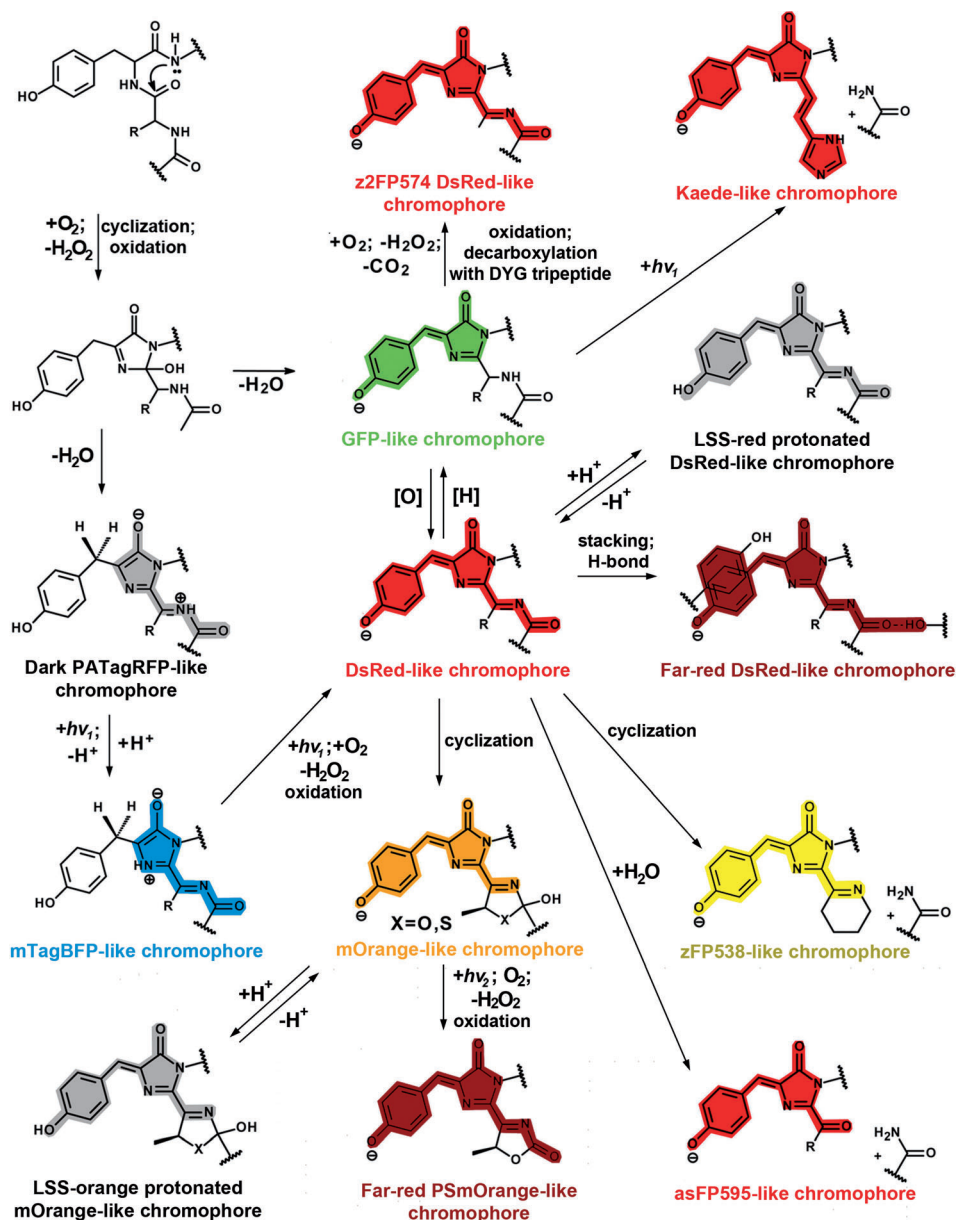

Figure 3. Mechanisms of chromophore formation for the DsRed-like, Kaede-like, mOrange-like, zFP538-like, asFP595-like, far-red DsRed-like, PSmOrange-like, LSS-red, and LSS-orange chromophores: Red, dark-red, orange, blue, green, and yellow colors of the chromophores correspond to the spectral range of the chromophore fluorescence. Gray denotes the non-fluorescent state. Transitions that can be photo-induced with 405 nm or 488 nm light are indicated by hv_1 and hv_2, respectively. [O] and [H] denote the oxidizing and reducing agents, respectively. Chromophores are shown in the *cis* form. Possible structures of *trans* chromophores and *cis*–*trans* isomerizations are not shown.

To date there are three major families of RFPs containing the DsRed-like chromophore: derivatives of DsRed,[101] eqFP578,[38] and eqFP611.[102] It was shown that the mechanism of the DsRed-like chromophore maturation first involves the formation of the N-acylimine C=N bond characteristic of the mTagBFP[103] chromophore, then the C^{α}–C^{β} double bond in the Tyr66 side chain is formed[2b, 99] (Figure 3). There is only one DsRed-like RFP that was shown to mature via the GFP-like chromophore intermediate.[2d] Studies of several FPs (dark-to-red PAmCherry,[2a] mCherry-based FTs,[2e] mTagBFP[103a], and mTagBFP2[103b]) with different phenotypes support the structure of the mTagBFP-like blue intermediate.

The red PAmCherry off (dark) state has the structure of the mTagBFP-like chromophore but without blue fluorescence.[2a] After irradiation with violet light, the PAmCherry dark chromophore photochemically converts into the red fluorescent DsRed-like state. PATagRFP in the dark state most likely has the structure of the mTagBFP-like chromophore precursor (Figure 3).[52] The mechanism of the reversible photoswitching has been studied for rsTagRFP.[94] It was found that a *cis–trans* isomerization of the DsRed-like chromophore accompanied by its protonation/deprotonation is responsible for the dark-fluorescent rsTagRFP cycling.

The second type of the red chromophore, Kaede-like (Figure 3), is found in the red state of green-to-red PSFPs.[2c] In the green state, these FPs have the GFP-like chromophore. After irradiation with violet light, green-to-red photoconversion occurs by a β-elimination reaction. In this process, a His65 N–C^{α} bond is cleaved and the C^{α}–C^{β} double bond in the His65 side chain is subsequently formed leading to an extension of the π-conjugated system and the resulting Kaede-like red chromophore.[2c]

Different color hues of FPs result from further transformations of the DsRed-like chromophore. The cyclization of the first amino acid in the chromophore with the C=N group or the carbonyl group of the N-acylimine leads to a yellow zFP538-like chromophore[2f] or to an orange mOrange-like chromophore,[2g] respectively (Figure 3). Irradiation of the mOrange-like chromophore with blue–green light, causes the photoinduced oxidation of the chromophore and subsequent cleavage of the polypeptide chain. As a result, the far-red PSmOrange-like chromophore containing N-acylimine with a co-planar carbon–oxygen double bond is formed.[37] Autocatalytic cleavage of the DsRed-like chromophore in the N-acylimine region in the related FP from *Anemonia sulcata* asFP595 results in the asFP595-like chromophore.[2h]

In RFPs with a large Stokes shift, such as LSSmKates[45] and mKeima,[44] the hydroxy group in the Tyr66 side chain of the DsRed-like chromophore is protonated (Figure 3). The initially protonated chromophore converts into the excited state on absorption of a photon. Then, the excited state proton transfer (ESPT) occurs from the hydroxy group of Tyr66 resulting in the anionic chromophore, which emits a red photon.[2i] The possibility to rationally design the LSS phenotype was demonstrated by engineering ESPT in a number of FPs.[2i] A switchable ESPT responding to changes

in pH value was developed as the single-FP biosensor pHRed,[104] which is based on mKeima.

Based on the available data on the structures of red chromophores, their derivatives, and transitions between them we can make the following conclusions. First, chemical transitions between the chromophore structures can either occur autocatalytically, be photoinduced, or be blocked. Second, a chromophore can be in a fluorescent state or in a chromo state (i.e., it absorbs but does not emit light). Third, amino acid residues in the chromophore and its microenvironment determine the transitions between the chromophore structures that result in the particular FP phenotypes.

Further studies, such as electronic structure calculations and chemical synthesis of model chromophores applied together with crystallography, mass-spectrometry, biochemical, and photophysical characterization should aid in further clarification of the chemical and spectral behavior of the FP chromophores. For instance, the synthesis of model compounds should confirm a specific chromophore structure among several variants suggested on the basis of structural or mass-spectrometry studies. It could also provide information on the influence of chemical groups participating in the chromophore formation on its spectral and photochemical characteristics.[2h, 100]

9. Outlook

The optimization of specific RFP properties for a particular imaging technique will improve the probe performance (Table 2). RFPs with increased brightness and enhanced photostability, particularly in the far-red spectral region, are highly desired.

Also in high demand are RFPs optimized for 2P excitation. Development of high-throughput approaches to screen large libraries of RFP mutants in 2P mode is required to achieve this goal.

PALM-based super-resolution imaging will benefit from PAFPs with improved single-molecule brightness and photostability. Another super-resolution approach, RESOLFT, has not yet reached its full potential in live-cell imaging with rsFPs as the probes. To acquire an image, the RESOLFT scanning requires a large number of switching cycles without loss of rsFP brightness. The recently reported photostable green rsEGFP provides a stimulus for the further development of RESOLFT imaging.[66] Future design of red rsFPs would add multicolor features to this technique. PALM and RESOLFT approaches could also benefit from the development of red rsFPs in which the fluorescence excitation is decoupled from the photoswitching, thus allowing a more controllable photomanipulation. This type of green rsFP, called Dreiklang, has been already engineered.[105]

There is a large demand for imaging approaches allowing multiple cellular events to be studied at the same time. In this regard spectrally resolvable orange, red, and far-red variants of FPs are required. LSSFPs should be useful in multicolor FRET, FCCS, and 2P microscopy. Designing ESPT in far-red FPs should result in far-red LSSFPs that can be combined with LSSmKate2 or LSSmOrange. It would also be useful to
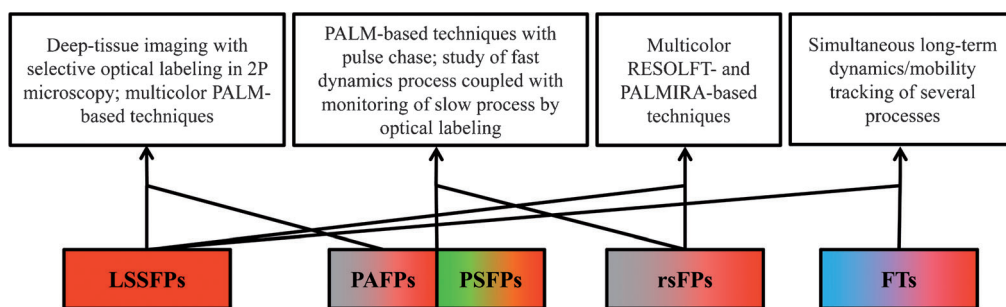
Figure 4. Possible applications of future RFPs with combined phenotypes. Different FP phenotypes are shown in the bottom row. Two phenotypes that can be combined in a single FP are connected with an arrow pointing to the imaging applications of the new resulting FP. Possible combinations of LSSFPs, PAFPs/PSFPs, rsFPs, and FTs are presented. The colors of the boxes correspond to different FP phenotypes and show the spectral range of chromophore fluorescence.

engineer an autocatalytic orange-to-far-red chromophore transformation that could result in a FT phenotype for deep-tissue imaging.

Further shifting of RFPs towards the infra-red part of spectrum will facilitate intravital microscopy and whole-body imaging. Although already implemented in bacterial phytochromes, which require biliverdin for fluorescence, infra-red FPs of the GFP protein family should be useful.

The available crystal structures of RFPs with the DsRed-like chromophore show that a C=O group of the N-acylimine is out of the chromophore plane.[2b,g] A red shift in FP excitation should be possible if the C=O group is coplanar with the chromophore, a feature that is found in the photoinduced far-red PSmOrange-like chromophore (Figure 3). Designing a probe with an autocatalytic formation of this type of the far-red chromophore could enable the imaging of animals in the NIRW region using GFP-like FPs.

Another FP design strategy is a combination of different FP phenotypes in a single protein. Emerging RFP variants and their respective applications are summarized in Figure 4. Not all FP properties can be combined. Only phenotypes with independent chromophore-transformation pathways could be joined (Figure 3). For example, since different amino acids are involved in the LSS and photoactivatable phenotypes, their merging would result in PA-LSSFPs.

To choose an optimal fluorescent probe, all the RFP's properties should be considered in their relation to the chosen microscopy technique, the biological object, and the experimental set-up. Future enhanced RFPs of existing and novel phenotypes will stimulate the development of novel imaging techniques to address a variety of challenges in biology.

[1] a) L. D. Lavis, R. T. Raines, *ACS Chem. Biol.* **2008**, *3*, 142–155; b) I. Johnson, M. T. Z. Spence, *The Molecular Probes Handbook: A Guide to Fluorescent Probes and Labeling Technologies*, 11th ed., Life Technologies Corp., USA, **2010**.

[2] a) F. V. Subach, V. N. Malashkevich, W. D. Zencheck, H. Xiao, G. S. Filonov, S. C. Almo, V. V. Verkhusha, *Proc. Natl. Acad. Sci. USA* **2009**, *106*, 21097–21102; b) O. M. Subach, V. N. Malashkevich, W. D. Zencheck, K. S. Morozova, K. D. Piatkevich, S. C. Almo, V. V. Verkhusha, *Chem. Biol.* **2010**, *17*, 333–341; c) H. Mizuno, T. K. Mal, K. I. Tong, R. Ando, T. Furuta, M. Ikura, A. Miyawaki, *Mol. Cell* **2003**, *12*, 1051–1058; d) A. A. Pakhomov, V. I. Martynov, *Biochemistry* **2007**, *46*, 11528–11535; e) S. Pletnev, F. V. Subach, Z. Dauter, A. Wlodawer, V. V. Verkhusha, *J. Am. Chem. Soc.* **2010**, *132*, 2243–2253; f) S. J. Remington, R. M. Wachter, D. K. Yarbrough, B. Branchaud, D. C. Anderson, K. Kallio, K. A. Lukyanov, *Biochemistry* **2005**, *44*, 202–212; g) X. Shu, N. C. Shaner, C. A. Yarbrough, R. Y. Tsien, S. J. Remington, *Biochemistry* **2006**, *45*, 9639–9647; h) I. V. Yampolsky, S. J. Remington, V. I. Martynov, V. K. Potapov, S. Lukyanov, K. A. Lukyanov, *Biochemistry* **2005**, *44*, 5788–5793; i) K. D. Piatkevich, V. N. Malashkevich, S. C. Almo, V. V. Verkhusha, *J. Am. Chem. Soc.* **2010**, *132*, 10762–10770.

[3] a) R. L. Strack, D. E. Strongin, D. Bhattacharyya, W. Tao, A. Berman, H. E. Broxmeyer, R. J. Keenan, B. S. Glick, *Nat. Methods* **2008**, *5*, 955–957; b) W. Tao, B. G. Evans, J. Yao, S. Cooper, K. Cornetta, C. B. Ballas, G. Hangoc, H. E. Broxmeyer, *Stem Cells* **2007**, *25*, 670–678.

[4] R. L. Strack, B. Hein, D. Bhattacharyya, S. W. Hell, R. J. Keenan, B. S. Glick, *Biochemistry* **2009**, *48*, 8279–8281.

[5] R. L. Strack, D. Bhattacharyya, B. S. Glick, R. J. Keenan, *BMC Biotechnol.* **2009**, *9*, 32.

[6] N. C. Shaner, M. Z. Lin, M. R. McKeown, P. A. Steinbach, K. L. Hazelwood, M. W. Davidson, R. Y. Tsien, *Nat. Methods* **2008**, *5*, 545–551.

[7] N. C. Shaner, R. E. Campbell, P. A. Steinbach, B. N. Giepmans, A. E. Palmer, R. Y. Tsien, *Nat. Biotechnol.* **2004**, *22*, 1567–1572.

[8] E. M. Merzlyak, J. Goedhart, D. Shcherbo, M. E. Bulina, A. S. Shcheglov, A. F. Fradkov, A. Gaintzeva, K. A. Lukyanov, S. Lukyanov, T. W. Gadella, D. M. Chudakov, *Nat. Methods* **2007**, *4*, 555–557.

[9] A. Sakaue-Sawano, H. Kurokawa, T. Morimura, A. Hanyu, H. Hama, H. Osawa, S. Kashiwagi, K. Fukami, T. Miyata, H. Miyoshi, T. Imamura, M. Ogawa, H. Masai, A. Miyawaki, *Cell* **2008**, *132*, 487–498.

[10] H. Tsutsui, S. Karasawa, Y. Okamura, A. Miyawaki, *Nat. Methods* **2008**, *5*, 683–685.

[11] S. Kredel, F. Oswald, K. Nienhaus, K. Deuschle, C. Rocker, M. Wolff, R. Heilker, G. U. Nienhaus, J. Wiedenmann, *PLoS One* **2009**, *4*, e4391.

[12] a) W. B. Frommer, M. W. Davidson, R. E. Campbell, *Chem. Soc. Rev.* **2009**, *38*, 2833–2841; b) A. Ibraheem, R. E. Campbell, *Curr. Opin. Chem. Biol.* **2010**, *14*, 30–36.

[13] a) H. J. Carlson, R. E. Campbell, *Curr. Opin. Biotechnol.* **2009**, *20*, 19–27; b) C. Schultz, A. Schleifenbaum, J. Goedhart, T. W. Gadella, Jr., *ChemBioChem* **2005**, *6*, 1323–1330.

[14] Y. Sun, C. F. Booker, S. Kumari, R. N. Day, M. Davidson, A. Periasamy, *J. Biomed. Opt.* **2009**, *14*, 054009.

[15] T. Nagai, S. Yamada, T. Tominaga, M. Ichikawa, A. Miyawaki, *Proc. Natl. Acad. Sci. USA* **2004**, *101*, 10554–10559.

[16] D. E. Johnson, H. W. Ai, P. Wong, J. D. Young, R. E. Campbell, J. R. Casey, *J. Biol. Chem.* **2009**, *284*, 20499–20511.

[17] Y. Zhao, S. Araki, J. Wu, T. Teramoto, Y. F. Chang, M. Nakano, A. S. Abdelfattah, M. Fujiwara, T. Ishihara, T. Nagai, R. E. Campbell, *Science* **2011**, *333*, 1888–1891.

[18] a) J. Y. Fan, Z. Q. Cui, H. P. Wei, Z. P. Zhang, Y. F. Zhou, Y. P. Wang, X. E. Zhang, *Biochem. Biophys. Res. Commun.* **2008**, *367*, 47–53; b) S. A. Davidson, R. H. Gilkey, H. S. Colburn, L. H. Carney, *J. Acoust. Soc. Am.* **2006**, *119*, 2258–2275.

[19] T. Sunabori, A. Tokunaga, T. Nagai, K. Sawamoto, M. Okabe, A. Miyawaki, Y. Matsuzaki, T. Miyata, H. Okano, *J. Cell Sci.* **2008**, *121*, 1204–1212.

[20] M. Sugiyama, A. Sakaue-Sawano, T. Iimura, K. Fukami, T. Kitaguchi, K. Kawakami, H. Okamoto, S. Higashijima, A. Miyawaki, *Proc. Natl. Acad. Sci. USA* **2009**, *106*, 20812–20817.

[21] J. Huisken, J. Swoger, F. Del Bene, J. Wittbrodt, E. H. Stelzer, *Science* **2004**, *305*, 1007–1009.

[22] A. H. Voie, D. H. Burns, F. A. Spelman, *J. Microsc.* **1993**, *170*, 229–236.

[23] M. Tokunaga, N. Imamoto, K. Sakata-Sogawa, *Nat. Methods* **2008**, *5*, 159–161.

[24] J. Huisken, D. Y. Stainier, *Development* **2009**, *136*, 1963–1975.

[25] a) B. G. Wang, K. Konig, K. J. Halbhuber, *J. Microsc.* **2010**, *238*, 1–20; b) W. Denk, J. H. Strickler, W. W. Webb, *Science* **1990**, *248*, 73–76; c) W. Denk, K. Svoboda, *Neuron* **1997**, *18*, 351–357.

[26] G. H. Patterson, D. W. Piston, *Biophys. J.* **2000**, *78*, 2159–2162.

[27] D. Entenberg, J. Wyckoff, B. Gligorijevic, E. T. Roussos, V. V. Verkhusha, J. W. Pollard, J. Condeelis, *Nat. Protoc.* **2011**, *6*, 1500–1520.

[28] M. Drobizhev, N. S. Makarov, S. E. Tillo, T. E. Hughes, A. Rebane, *Nat. Methods* **2011**, *8*, 393–399.

[29] B. Hein, K. I. Willig, S. W. Hell, *Proc. Natl. Acad. Sci. USA* **2008**, *105*, 14271–14276.

[30] A. M. Smith, M. C. Mancini, S. Nie, *Nat. Nanotechnol.* **2009**, *4*, 710–711.

[31] M. Z. Lin, M. R. McKeown, H. L. Ng, T. A. Aguilera, N. C. Shaner, R. E. Campbell, S. R. Adams, L. A. Gross, W. Ma, T. Alber, R. Y. Tsien, *Chem. Biol.* **2009**, *16*, 1169–1179.

[32] K. S. Morozova, K. D. Piatkevich, T. J. Gould, J. Zhang, J. Bewersdorf, V. V. Verkhusha, *Biophys. J.* **2010**, *99*, L13–15.

[33] D. Shcherbo, I. I. Shemiakina, A. V. Ryabova, K. E. Luker, B. T. Schmidt, E. A. Souslova, T. V. Gorodnicheva, L. Strukova, K. M. Shidlovskiy, O. V. Britanova, A. G. Zaraisky, K. A. Lukyanov, V. B. Loschenov, G. D. Luker, D. M. Chudakov, *Nat. Methods* **2010**, *7*, 827–829.

[34] X. Shu, A. Royant, M. Z. Lin, T. A. Aguilera, V. Lev-Ram, P. A. Steinbach, R. Y. Tsien, *Science* **2009**, *324*, 804–807.

[35] G. S. Filonov, K. D. Piatkevich, L. M. Ting, J. Zhang, K. Kim, V. V. Verkhusha, *Nat. Biotechnol.* **2011**, *29*, 757–761.

[36] N. C. Deliolanis, R. Kasmieh, T. Wurdinger, B. A. Tannous, K. Shah, V. Ntziachristos, *J. Biomed. Opt.* **2008**, *13*, 044008.

[37] O. M. Subach, G. H. Patterson, L. M. Ting, Y. Wang, J. S. Condeelis, V. V. Verkhusha, *Nat. Methods* **2011**, *8*, 771–777.

[38] D. Shcherbo, E. M. Merzlyak, T. V. Chepurnykh, A. F. Fradkov, G. V. Ermakova, E. A. Solovieva, K. A. Lukyanov, E. A.

[39] R. Diéguez-Hurtado, J. Martín, I. Martínez-Corral, M. D. Martínez, D. Megías, D. Olmeda, S. Ortega, *Genesis* **2011**, *49*, 36–45.

[40] S. W. Hell, J. Wichmann, *Opt. Lett.* **1994**, *19*, 780–782.

[41] O. Zapata-Hommer, O. Griesbeck, *BMC Biotechnol.* **2003**, *3*, 5.

[42] H. W. Ai, K. L. Hazelwood, M. W. Davidson, R. E. Campbell, *Nat. Methods* **2008**, *5*, 401–403.

[43] D. M. Shcherbakova, M. A. Hink, L. Joosen, T. J. Gadella, Jr., V. V. Verkhusha, *J. Am. Chem. Soc.* **2012**, *134*, 7913–7923..

[44] T. Kogure, S. Karasawa, T. Araki, K. Saito, M. Kinjo, A. Miyawaki, *Nat. Biotechnol.* **2006**, *24*, 577–581.

[45] K. D. Piatkevich, J. Hulit, O. M. Subach, B. Wu, A. Abdulla, J. E. Segall, V. V. Verkhusha, *Proc. Natl. Acad. Sci. USA* **2010**, *107*, 5369–5374.

[46] K. Bacia, S. A. Kim, P. Schwille, *Nat. Methods* **2006**, *3*, 83–89.

[47] H. Kawano, T. Kogure, Y. Abe, H. Mizuno, A. Miyawaki, *Nat. Methods* **2008**, *5*, 373–374.

[48] D. Shcherbo, C. S. Murphy, G. V. Ermakova, E. A. Solovieva, T. V. Chepurnykh, A. S. Shcheglov, V. V. Verkhusha, V. Z. Pletnev, K. L. Hazelwood, P. M. Roche, S. Lukyanov, A. G. Zaraisky, M. W. Davidson, D. M. Chudakov, *Biochem. J.* **2009**, *418*, 567–574.

[49] F. V. Subach, O. M. Subach, I. S. Gundorov, K. S. Morozova, K. D. Piatkevich, A. M. Cuervo, V. V. Verkhusha, *Nat. Chem. Biol.* **2009**, *5*, 118–126.

[50] T. Tsuboi, T. Kitaguchi, S. Karasawa, M. Fukuda, A. Miyawaki, *Mol. Biol. Cell* **2010**, *21*, 87–94.

[51] F. V. Subach, G. H. Patterson, S. Manley, J. M. Gillette, J. Lippincott-Schwartz, V. V. Verkhusha, *Nat. Methods* **2009**, *6*, 153–159.

[52] F. V. Subach, G. H. Patterson, M. Renz, J. Lippincott-Schwartz, V. V. Verkhusha, *J. Am. Chem. Soc.* **2010**, *132*, 6481–6491.

[53] M. S. Gunewardene, F. V. Subach, T. J. Gould, G. P. Penoncello, M. V. Gudheti, V. V. Verkhusha, S. T. Hess, *Biophys. J.* **2011**, *101*, 1522–1528.

[54] D. M. Chudakov, S. Lukyanov, K. A. Lukyanov, *Nat. Protoc.* **2007**, *2*, 2024–2032.

[55] S. A. McKinney, C. S. Murphy, K. L. Hazelwood, M. W. Davidson, L. L. Looger, *Nat. Methods* **2009**, *6*, 131–133.

[56] a) S. Habuchi, H. Tsutsui, A. B. Kochaniak, A. Miyawaki, A. M. van Oijen, *PLoS One* **2008**, *3*, e3944; b) H. Hoi, N. C. Shaner, M. W. Davidson, C. W. Cairo, J. Wang, R. E. Campbell, *J. Mol. Biol.* **2010**, *401*, 776–791.

[57] J. Fuchs, S. Bohme, F. Oswald, P. N. Hedde, M. Krause, J. Wiedenmann, G. U. Nienhaus, *Nat. Methods* **2010**, *7*, 627–630.

[58] K. B. Bravaya, B. L. Grigorenko, A. V. Nemukhin, A. I. Krylov, *Acc. Chem. Res.* **2012**, *45*, 265–275.

[59] A. C. Stiel, M. Andresen, H. Bock, M. Hilbert, J. Schilde, A. Schonle, C. Eggeling, A. Egner, S. W. Hell, S. Jakobs, *Biophys. J.* **2008**, *95*, 2989–2997.

[60] F. V. Subach, L. Zhang, T. W. Gadella, N. G. Gurskaya, K. A. Lukyanov, V. V. Verkhusha, *Chem. Biol.* **2010**, *17*, 745–755.

[61] a) G. T. Hanson, T. B. McAnaney, E. S. Park, M. E. Rendell, D. K. Yarbrough, S. Chu, L. Xi, S. G. Boxer, M. H. Montrose, S. J. Remington, *Biochemistry* **2002**, *41*, 15477–15488; b) J. R. Moore, S. A. Davidson, M. Singh, *Gynecol. Oncol.* **2004**, *95*, 729–732.

[62] D. M. Chudakov, V. V. Verkhusha, D. B. Staroverov, E. A. Souslova, S. Lukyanov, K. A. Lukyanov, *Nat. Biotechnol.* **2004**, *22*, 1435–1439.

[63] J. Wiedenmann, S. Ivanchenko, F. Oswald, F. Schmitt, C. Rocker, A. Salih, K. D. Spindler, G. U. Nienhaus, *Proc. Natl. Acad. Sci. USA* **2004**, *101*, 15905–15910.

[64] V. Adam, M. Lelimousin, S. Boehme, G. Desfonds, K. Nienhaus, M. J. Field, J. Wiedenmann, S. McSweeney, G. U.

Bogdanova, A. G. Zaraisky, S. Lukyanov, D. M. Chudakov, *Nat. Methods* **2007**, *4*, 741–746.

Nienhaus, D. Bourgeois, *Proc. Natl. Acad. Sci. USA* **2008**, *105*, 18343 – 18348.

[65] E. Betzig, G. H. Patterson, R. Sougrat, O. W. Lindwasser, S. Olenych, J. S. Bonifacino, M. W. Davidson, J. Lippincott-Schwartz, H. F. Hess, *Science* **2006**, *313*, 1642 – 1645.

[66] T. Grotjohann, I. Testa, M. Leutenegger, H. Bock, N. T. Urban, F. Lavoie-Cardinal, K. I. Willig, C. Eggeling, S. Jakobs, S. W. Hell, *Nature* **2011**, *478*, 204 – 208.

[67] a) S. W. Hell, *Science* **2007**, *316*, 1153 – 1158; b) S. W. Hell, *Nat. Methods* **2009**, *6*, 24 – 32; c) B. Huang, H. Babcock, X. Zhuang, *Cell* **2010**, *143*, 1047 – 1058.

[68] T. A. Klar, S. W. Hell, *Opt. Lett.* **1999**, *24*, 954 – 956.

[69] S. W. Hell, M. Kroug, *Appl. Phys. B* **1995**, *60*, 495 – 497.

[70] S. W. Hell, *Nat. Biotechnol.* **2003**, *21*, 1347 – 1355.

[71] M. Hofmann, C. Eggeling, S. Jakobs, S. W. Hell, *Proc. Natl. Acad. Sci. USA* **2005**, *102*, 17565 – 17569.

[72] P. Kner, B. B. Chhun, E. R. Griffis, L. Winoto, M. G. Gustafsson, *Nat. Methods* **2009**, *6*, 339 – 342.

[73] M. Andresen, A. C. Stiel, J. Folling, D. Wenzel, A. Schonle, A. Egner, C. Eggeling, S. W. Hell, S. Jakobs, *Nat. Biotechnol.* **2008**, *26*, 1035 – 1040.

[74] J. C. Vaughan, X. Zhuang, *Nat. Biotechnol.* **2011**, *29*, 880 – 881.

[75] S. T. Hess, T. P. Girirajan, M. D. Mason, *Biophys. J.* **2006**, *91*, 4258 – 4272.

[76] M. Bates, B. Huang, G. T. Dempsey, X. Zhuang, *Science* **2007**, *317*, 1749 – 1753.

[77] M. Heilemann, S. van de Linde, M. Schuttpelz, R. Kasper, B. Seefeldt, A. Mukherjee, P. Tinnefeld, M. Sauer, *Angew. Chem.* **2008**, *120*, 6266 – 6271; *Angew. Chem. Int. Ed.* **2008**, *47*, 6172 – 6176.

[78] J. Fölling, M. Bossi, H. Bock, R. Medda, C. A. Wurm, B. Hein, S. Jakobs, C. Eggeling, S. W. Hell, *Nat. Methods* **2008**, *5*, 943 – 945.

[79] D. T. Burnette, P. Sengupta, Y. Dai, J. Lippincott-Schwartz, B. Kachar, *Proc. Natl. Acad. Sci. USA* **2011**, *108*, 21081 – 21086.

[80] A. G. York, A. Ghitani, A. Vaziri, M. W. Davidson, H. Shroff, *Nat. Methods* **2011**, *8*, 327 – 333.

[81] G. Shtengel, J. A. Galbraith, C. G. Galbraith, J. Lippincott-Schwartz, J. M. Gillette, S. Manley, R. Sougrat, C. M. Waterman, P. Kanchanawong, M. W. Davidson, R. D. Fetter, H. F. Hess, *Proc. Natl. Acad. Sci. USA* **2009**, *106*, 3125 – 3130.

[82] T. J. Gould, M. S. Gunewardene, M. V. Gudheti, V. V. Verkhusha, S. R. Yin, J. A. Gosse, S. T. Hess, *Nat. Methods* **2008**, *5*, 1027 – 1030.

[83] C. Flors, J. Hotta, H. Uji-i, P. Dedecker, R. Ando, H. Mizuno, A. Miyawaki, J. Hofkens, *J. Am. Chem. Soc.* **2007**, *129*, 13970 – 13977.

[84] S. T. Hess, T. J. Gould, M. V. Gudheti, S. A. Maas, K. D. Mills, J. Zimmerberg, *Proc. Natl. Acad. Sci. USA* **2007**, *104*, 17370 – 17375.

[85] M. J. Rust, M. Bates, X. Zhuang, *Nat. Methods* **2006**, *3*, 793 – 795.

[86] a) A. Egner, C. Geisler, C. von Middendorff, H. Bock, D. Wenzel, R. Medda, M. Andresen, A. C. Stiel, S. Jakobs, C. Eggeling, A. Schonle, S. W. Hell, *Biophys. J.* **2007**, *93*, 3285 – 3290; b) see Ref. [59].

[87] a) M. Tomura, N. Yoshida, J. Tanaka, S. Karasawa, Y. Miwa, A. Miyawaki, O. Kanagawa, *Proc. Natl. Acad. Sci. USA* **2008**, *105*, 10871 – 10876; b) D. Kedrin, B. Gligorijevic, J. Wyckoff, V. V. Verkhusha, J. Condeelis, J. E. Segall, J. van Rheenen, *Nat. Methods* **2008**, *5*, 1019 – 1021; c) S. L. Griswold, K. C. Sajja, C. W. Jang, R. R. Behringer, *Genesis* **2011**, *49*, 591 – 598; d) S. Nowotschin, A. K. Hadjantonakis, *BMC Dev. Biol.* **2009**, *9*, 49.

[88] A. Dovas, B. Gligorijevic, X. Chen, D. Entenberg, J. Condeelis, D. Cox, *PLoS One* **2011**, *6*, e16485.

[89] F. Cella Zanacchi, Z. Lavagnino, M. Perrone Donnorso, A. Del Bue, L. Furia, M. Faretta, A. Diaspro, *Nat. Methods* **2011**, *8*, 1047 – 1049.

[90] G. U. Nienhaus, K. Nienhaus, A. Holzle, S. Ivanchenko, F. Renzi, F. Oswald, M. Wolff, F. Schmitt, C. Rocker, B. Vallone, W. Weidemann, R. Heilker, H. Nar, J. Wiedenmann, *Photochem. Photobiol.* **2006**, *82*, 351 – 358.

[91] H. Shroff, C. G. Galbraith, J. A. Galbraith, H. White, J. Gillette, S. Olenych, M. W. Davidson, E. Betzig, *Proc. Natl. Acad. Sci. USA* **2007**, *104*, 20308 – 20313.

[92] P. Kanchanawong, G. Shtengel, A. M. Pasapera, E. B. Ramko, M. W. Davidson, H. F. Hess, C. M. Waterman, *Nature* **2010**, *468*, 580 – 584.

[93] T. A. Brown, A. N. Tkachuk, G. Shtengel, B. G. Kopek, D. F. Bogenhagen, H. F. Hess, D. A. Clayton, *Mol. Cell Biol.* **2011**, *31*, 4994 – 5010.

[94] S. Pletnev, F. V. Subach, Z. Dauter, A. Wlodawer, V. V. Verkhusha, *J. Mol. Biol.* **2012**, *417*, 144 – 151.

[95] M. A. Schwentker, H. Bock, M. Hofmann, S. Jakobs, J. Bewersdorf, C. Eggeling, S. W. Hell, *Microsc. Res. Tech.* **2007**, *70*, 269 – 280.

[96] a) see Ref. [2b]; b) see Ref. [2e].

[97] J. N. Henderson, M. F. Osborn, N. Koon, R. Gepshtein, D. Huppert, S. J. Remington, *J. Am. Chem. Soc.* **2009**, *131*, 13212 – 13213.

[98] X. Shu, L. Wang, L. Colip, K. Kallio, S. J. Remington, *Protein Sci.* **2009**, *18*, 460 – 466.

[99] K. B. Bravaya, O. M. Subach, N. Korovina, V. V. Verkhusha, A. I. Krylov, *J. Am. Chem. Soc.* **2012**, *134*, 2807 – 2814.

[100] a) I. V. Yampolsky, A. A. Kislukhin, T. T. Amatov, D. Shcherbo, V. K. Potapov, S. Lukyanov, K. A. Lukyanov, *Bioorg. Chem.* **2008**, *36*, 96 – 104; b) I. V. Yampolsky, T. A. Balashova, K. A. Lukyanov, *Biochemistry* **2009**, *48*, 8077 – 8082.

[101] L. A. Gross, G. S. Baird, R. C. Hoffman, K. K. Baldridge, R. Y. Tsien, *Proc. Natl. Acad. Sci. USA* **2000**, *97*, 11990 – 11995.

[102] J. Petersen, P. G. Wilmann, T. Beddoe, A. J. Oakley, R. J. Devenish, M. Prescott, J. Rossjohn, *J. Biol. Chem.* **2003**, *278*, 44626 – 44631.

[103] a) O. M. Subach, I. S. Gundorov, M. Yoshimura, F. V. Subach, J. Zhang, D. Gruenwald, E. A. Souslova, D. M. Chudakov, V. V. Verkhusha, *Chem. Biol.* **2008**, *15*, 1116 – 1124; b) O. M. Subach, P. J. Cranfill, M. W. Davidson, V. V. Verkhusha, *PLoS One* **2011**, *6*, e28674.

[104] M. Tantama, Y. P. Hung, G. Yellen, *J. Am. Chem. Soc.* **2011**, *133*, 10034 – 10037.

[105] T. Brakemann, A. C. Stiel, G. Weber, M. Andresen, I. Testa, T. Grotjohann, M. Leutenegger, U. Plessmann, H. Urlaub, C. Eggeling, M. C. Wahl, S. W. Hell, S. Jakobs, *Nat. Biotechnol.* **2011**, *29*, 942 – 947.